Proceedings of the ASME 2013 International Mechanical Engineering Congress and Exposition
IMECE2013
November 15-21, 2013, San Diego, California, USA

IMECE2013-63301

SIMPLE MECHANISTICALLY CONSISTENT FORMULATION FOR VOLUME-OF-FLUID BASED COMPUTATIONS OF CONDENSING FLOWS

Alexander S Rattner Alex.Rattner@gatech.edu
Srinivas Garimella* sgarimella@gatech.edu
G.W. Woodruff School of Mechanical Engineering
Georgia Institute of Technology
Atlanta, Georgia, USA

ABSTRACT

Numerous investigations have been conducted to extend adiabatic liquid-gas VOF flow solvers to include condensation phenomena by adding an energy equation and phase-change source terms. Some proposed phase-change models employ empirical rate parameters, or adapt heat transfer correlations, and thus must be tuned for specific applications. Generally applicable models have also been developed that rigorously resolve the phase-change process, but require interface reconstruction, significantly increasing computational cost and software complexity. In the present work, a simplified first-principles-based condensation model is developed, which forces interface-containing mesh cells to the equilibrium state. The operation on cells instead of complex interface surfaces enables the use of fast graph algorithms without reconstruction. The model is validated for horizontal film condensation, and converges to exact solutions with increasing mesh resolution. Agreement with established results is demonstrated for smooth and wavy falling-film condensation.

INTRODUCTION

Background

Condensation is a crucial and often limiting component of many energy intensive processes such as power generation, refrigeration, and materials manufacturing. Simple and sufficiently accurate analytical solutions and correlations exist for basic configurations, such as falling liquid films on flat plates and annular flow in round tubes. Advanced condenser designs could significantly reduce device size and pressure drop [1, 2]. However, the complex flow patterns in such devices cannot be predicted reliably with analytical or simplified models, and iterative, experimentally-based device design and optimization is often prohibitively expensive. Thus, substantial research efforts have been applied to the development of computational tools that can fully resolve and simulate condensing flows under complex operating conditions and geometries.

Literature Review

Mature commercially ([3-5]) and freely available [6] software tools have been developed for simulating two-phase liquid-gas flows without phase change. Most of these programs track the development of the fluid phases with a Lagrangian (i.e. transported by the velocity field) phase-fraction field: α, that ideally varies from zero in the vapor phase to one in the liquid phase. In the *Volume-of-Fluid* (VOF) formulation [7], the local material properties are weighted by α, yielding a single set of governing equations valid for an entire simulation domain. Such VOF simulation frameworks can be extended to account for phase change by incorporating source and sink terms in the phase, momentum, continuity/pressure, and energy equations. Multiple formulations have been proposed for the phase change terms in these models, including: (1) empirical rate parameters, (2) adaptation of experimentally developed heat transfer correlations, and (3) direct evaluation of interfacial transport rates.

Empirical rate parameter based models

Yang et al. [8] performed simulations and experimental investigations of flow boiling of R141b in a horizontal tube. Their simulations employed compressible momentum and continuity equations, and coupled phase-change source terms were added to the phase and thermal energy transport equations. Geometric interface reconstruction was performed using the piecewise-linear approach implemented in FLUENT [3]. The rate of phase change (S, kg m^{-3} s^{-1}) at the interface was controlled with an empirical rate parameter r (s^{-1}).

*Corresponding author

$$S = \begin{cases} r\alpha\rho_{\mathrm{L}} \dfrac{T - T_{\mathrm{sat}}}{T_{\mathrm{sat}}} & T \geq T_{\mathrm{sat}} \\ r(1-\alpha)\rho_{\mathrm{v}} \dfrac{T - T_{\mathrm{sat}}}{T_{\mathrm{sat}}} & T < T_{\mathrm{sat}} \end{cases} \quad (1)$$

Yang et al. found that a value of r = 100 s^{-1} was sufficient to maintain the interface within 1 K of the saturation temperature without introducing large numerical oscillations. However, r acts as a surrogate for the *characteristic* thermal time scale of mesh cells ($\tau_{\mathrm{cell}} = \rho c_{\mathrm{p}} \Delta x^2 / k$), and should therefore depend on the simulation mesh resolution and fluid properties.

Fang et al. [9] simulated boiling flows in a *vapor venting microchannel*, in which a semipermeable membrane permitted vapor removal to improve heat transfer performance and reduce frictional losses. In this investigation, coupled terms were introduced to the phase and energy equations to account for phase change, but no modifications were made to the momentum or continuity equations to account for volume generation from boiling. Fang et al. adopted the phase-change rate parameter model of Yang et al [9], but selected the same value for r (100 s^{-1}) even though they used a much finer mesh resolution and a different working fluid (water).

Thiele [10] employed a similar rate-parameter-based approach for modeling horizontal film condensation, and applied a limiting condition to ensure that the amount of vapor condensed per time step did not exceed the amount present in the cells. It was shown that the rate parameter approach with fixed r did not yield convergent results with increasing mesh resolution. Again, this can be attributed to the fact that the characteristic thermal time scale of a mesh cell (τ_{cell}) depends on its size.

Analytical solution and correlation based models

Jeon et al. [11] simulated the condensation of a rising vapor bubble in a liquid medium using the VOF approach. Phase change source terms were introduced to the phase fraction and energy equations, but the momentum and continuity equations were not modified to account for the volumetric reduction due to condensation. The condensation rate was modeled by applying the convection coefficient from the correlation of Kim and Park [12] at the interface. This approach has the advantage of incorporating experimentally validated data into the model description, but limits applicability to simulations with similar phase change conditions. Additionally, the use of an average heat transfer coefficient over the entire bubble surface limits the accuracy of a CFD simulation, in which local interface temperature gradients may vary significantly.

Thiele [10] adapted the Nusselt flat-plate falling-film condensation solution [13] into a form applicable to individual mesh cells. Thiele implemented his model in the OpenFOAM® interFoam framework [14]. No interface reconstruction is performed in interFoam, reducing computational cost and simplifying support of unstructured meshes. Rather, a compressive velocity field is superimposed in the vicinity of the interface to reduce numerical diffusion (based on [14, 15]). Because interfacial geometry data were not available, Thiele developed a simplified model in which the assumed interface area in each cell scales with α, approaching 0 at α = 0,1 and a maximal value at α = 0.5. This approach was shown to achieve grid independence for a horizontal condensing film simulation. However, the applicability of this approach to general condensation configurations is unclear.

Interfacial transport based models

Bothe and Warnecke [16] developed a computational model to study mass transfer from rising gas bubbles in a liquid medium. While technically an adiabatic absorption process, this problem is closely related to condensation. In this investigation, mass transfer across the interface was modeled by applying an equilibrium concentration to interface cells, and solving the species transport equation throughout the domain. The interface itself was reconstructed using the piecewise linear interface calculation (PLIC) method [17].

Subramaniam and Garimella [18] performed 2D and 3D simulations of falling lithium bromide-water films over cooled horizontal tubes in a water vapor atmosphere, as would be employed in the absorber component of an absorption chiller. As in the study by Bothe and Warnecke [16], the interface was reconstructed using the PLIC method, and phase-change mass transfer rates were determined by solving the species transport equation directly. They also employed a thermal energy equation to account for coupled heat and mass transfer effects. Both these studies neglected volumetric and velocity changes due to phase change.

Marschall et al. [19] also investigated the problem of mass transfer across liquid-gas interfaces, but implemented their models in the OpenFOAM® interFoam framework. Because geometric interface data were not available, Marschall et al. implemented a continuum species transport (CST) model applied to interface cells, analogous to the widely used continuum surface-tension force (CSF) model [20].

Juric and Tryggvason [21] implemented a model in which the effects of the interface (surface tension, phase change heating and volumetric fluxes, etc.) are applied to the discretized equations as smoothed delta functions. The actual interface is modeled as connected points overlaid on the main simulation mesh that are advected at each time step in a combined Lagrangian/Eulerian formulation. This approach increases program complexity, but avoids any numerical diffusion of the interface and allows direct evaluation of interfacial transport quantities. They validated their model for 1-D evaporation, and grid-independence was demonstrated. Two-dimensional film-boiling simulations were also performed. In a follow-on study, Esmaeeli and Tryggvason [22] extended this model to support 3D simulations on structured rectilinear grids. Validation studies were performed for falling liquid films, the Rayleigh-Taylor instability with heat and mass transfer, evaporation of a superheated liquid film, and film boiling. These simulations were shown to achieve grid

independence, and close agreement with experimental and analytical results was obtained.

Tao et al. [23] investigated bubble growth in liquid films, motivated by the application of water spray cooling. Their model accounted for volumetric generation during boiling and the associated momentum source. The phase change rate was determined based on the difference of normal heat fluxes across the interface; therefore, geometric reconstruction was presumably performed. However, no phase-change term was applied to the phase transport equation. Results were reported for the growth and detachment of a 2D bubble and associated surface heat transfer.

Zhang et al. [24] investigated film boiling using an approach based on that developed by Esmaeeli and Tryggvason [22], in which the interface is reconstructed using the PLIC algorithm and directly advected. The phase change rate is determined by directly evaluating the normal conduction heat transfer rates on both sides of the liquid-vapor interface. The actual interface velocity is calculated from a mass balance across the interface ($\rho_L\left(\bar{u}_{n,L}-\bar{u}_{int}\right)=\rho_V\left(\bar{u}_{n,V}-\bar{u}_{int}\right)$). A full 3D simulation was performed for the growth, necking, and break-off of a single vapor bubble. A number of simplifications were employed in this study, such as assuming a linear temperature profile from the wall to the interface (at T_{sat}), and material properties and operating conditions were selected to model a non-physical fluid with relatively small differences between the liquid and vapor phases and weak dynamic effects (ρ_V/ρ_L = 0.1, μ_V/μ_L = 0.1, Re = 1, Ja = 0.1).

Present Work

Based on the reviewed investigations, the most successfully validated phase change models for VOF simulations perform detailed evaluations of interfacial heat and mass transfer. However, such models have relied on geometric interface reconstruction or direct tracking and advection of the interface, which are both computationally expensive and difficult to perform on unstructured meshes. An alternative approach is investigated in the present study in which cells containing the interface are identified using a relatively simple and fast graph traversal algorithm. Condensation phase change source terms are then applied to such *interface cells*, similar to the CST formulation [19], without the need for geometric reconstruction. Interface cells are forced to the equilibrium state instantaneously, similar to rate parameter methods [8-10], but in a dynamic fashion that yields mesh independence. The method developed here is validated for horizontal film condensation and for smooth and wavy falling film condensation.

MODEL DEVELOPMENT

Governing Equations

Simulation of condensation problems in the VOF approach requires solution of the governing mass, momentum, energy, and phase equations. In this model, the incompressible continuity equation is modified with a source term ($\dot{v}_{pc}$) representing the volumetric generation per unit volume due to phase change. In actuality, condensing flows are compressible. However, the full compressible form of the continuity equation is not necessary because the densities of the liquid and vapor phases are assumed constant. Rather, a *volume transport equation* is employed.

$$\frac{\partial u_i}{\partial x_i}=\dot{v}_{pc} \tag{2}$$

The momentum equation is formulated neglecting compressibility effects. An effective viscosity (μ_{eff}) is employed, which could incorporate an eddy viscosity for turbulent flow simulations. Surface tension and the net gravitational forces are incorporated into a term *f*, following the interFoam formulation [14]. Surface tension is obtained without reconstruction by estimating local curvature and interface orientation using differential operations on the phase field α [25].

$$\vec{f}=-\left(\nabla\rho\right)\vec{g}\cdot\vec{x}+\sigma\left[\nabla\cdot\left(\frac{\nabla\alpha}{|\nabla\alpha|}\right)\right]\nabla\alpha \tag{3}$$

The complete momentum equation is formulated using $p_{\rho gh}$ – the pressure field without the hydrostatic component.

$$\rho\frac{\partial u_i}{\partial t}+\rho u_j\frac{\partial u_i}{\partial x_j}-\mu_{eff}\frac{\partial u_i}{\partial x_j\partial x_j}=-\frac{\partial p_{\rho gh}}{\partial x_i}+f_i \tag{4}$$

A simplified thermal energy transport equation is employed in which viscous dissipation and pressure transport terms are assumed negligible compared to the large convective and conduction heat fluxes typically encountered during condensation. As in the momentum equation, an effective conductivity ($(k/\rho)_{eff}$) is employed to permit incorporation of eddy diffusivity for turbulent flow simulations. A volumetric heat source term ($\dot{q}_{pc}$) is included to account for the latent heat released during condensation.

$$\frac{\partial h}{\partial t}+\frac{\partial}{\partial x_i}\left(u_i h\right)=\frac{\partial}{\partial x_i}\left[\left(\frac{k}{\rho}\right)_{eff}\frac{\partial T}{\partial x_i}\right]-\dot{q}_{pc} \tag{5}$$

Finally, the hyperbolic phase transport equation is modified with a generation term to account for the change in liquid volume fraction due to condensation ($\dot{\alpha}_{pc}$). The modified velocity field (u^*) includes corrections based on the gradient of the phase field to compress the interface and counteract numerical diffusion [14].

$$\frac{\partial\alpha}{\partial t}+\frac{\partial}{\partial x_i}\left(u_i^*\alpha\right)=\dot{\alpha}_{pc} \tag{6}$$

These governing equations are discretized with the OpenFOAM® library following the finite volume approach, and evaluated using the solution procedure described in the Algorithm Implementation section.

Material Properties

Thermophysical material properties are evaluated for each mesh cell. Surface tension (σ) and the phase change enthalpy (h_{LV}) are assumed uniform. The fluid density (ρ), viscosity (μ),

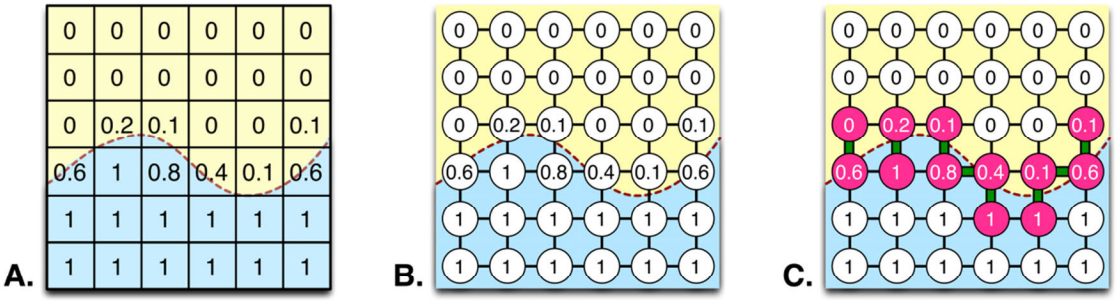

FIG. 1 – INTERFACE CELL IDENTIFICATION PROCESS: THE PHASE FRACTION FIELD ON MESH CELLS (A) YIELDS A GRAPH (B) FROM WHICH CELL PAIRS STRADDLING α = 0.5 FORM THE INTERFACE (C)

and thermal conductivity (k) are defined to be the volume weighted fraction average of the liquid and vapor phases.

$$\theta = \alpha\theta_{\mathrm{L}} + (1-\alpha)\theta_{\mathrm{V}} \qquad \theta \in [\rho, \mu, k] \tag{7}$$

A more precise model would evaluate the effective viscosity and thermal conductivity depending on the gradient of the phase field (i.e. whether the transport resistances of the two phases act in series or in parallel) [19]. However, such corrections are not significant provided the simulation mesh is sufficiently fine in the neighborhood of the interface, which is required for other reasons in the proposed phase change model (described in the following sections).

The specific heat of the fluid is evaluated using a mass-weighted average.

$$c_{\mathrm{p}} = \frac{\alpha\rho_{\mathrm{L}}c_{\mathrm{p,L}} + (1-\alpha)\rho_{\mathrm{V}}c_{\mathrm{p,V}}}{\rho} \tag{8}$$

The liquid and vapor specific heats are assumed constant in the present investigation; therefore, the fluid enthalpy can be related to temperature as:

$$h = (T - T_{\mathrm{sat}})c_{\mathrm{p}} \tag{9}$$

The enthalpy of phase change is not included in the above expression because it is accounted for in $\dot{q}_{\mathrm{pc}}$.

Phase Change Model

The phase change model developed here operates on mesh connectivity and volumetric field data, which are readily available in the OpenFOAM® implementation environment, and thus does not require geometric interface reconstruction.

At the beginning of the simulation, a graph of the mesh is formed where nodes and edges correspond to mesh cells and cell faces, respectively. During each time step, a scan is performed over the graph edges. Any *cell pairs* with phase field (α) values straddling an interface threshold value (typically α_{int} = 0.5) are added to an interface cell set. This interface cell identification process is summarized graphically in Fig. 1.

Condensation is physically a localized process acting on a nearly infinitesimally thin interface. However, without geometric reconstruction, it is not possible to identify precisely which cells are intersected by the interface, but only which *cell pairs* straddle the interface. Additionally, this approach supports common initial conditions where adjacent cells have phase values of α = 0 and α = 1 (i.e. for adjacent vapor and liquid regions), causing the interface to be coplanar with a cell face.

Defining *cell pairs* to contain the interface is consistent with the notion of an infinitesimally thin interface in the sense that, as the mesh is refined, the total volume of the interface cells approaches 0. Thus, this phase-change model requires a sufficiently fine mesh in the neighborhood of the interface. Cells with a *wall* boundary condition on a face are also added to the interface set, enabling direct condensation on walls.

Next, an initial non-limited volumetric phase change heating rate is evaluated for interface cells.

$$\dot{q}_{\mathrm{pc},0} = \frac{\rho c_{\mathrm{p}}(T - T_{\mathrm{sat}})}{\Delta t} \tag{10}$$

This approach resembles the empirical rate parameter model employed in [8-10]. However, here the phase change heating rate is defined to force the interface to the saturation temperature at *every* time step, recovering the physical equilibrium condition. In [8-10], the rate parameter was fixed and was independent of the simulation time step size, so the interface temperature could diverge from the saturation temperature. Conceptually, the present model assumes that the interface cells reach the equilibrium condition instantaneously, and thus have negligible internal heat transfer resistance and characteristic thermal time scales of τ_{cell} = 0. Again, this approach is valid, provided that the mesh is sufficiently fine in the neighborhood of the interface, so that the interface cells contribute a minor portion to the total condensation heat transfer resistance.

Limiting must be applied to the obtained phase change heating rate (Eqn. 10). To ensure physical results, the mass of fluid condensed in a mesh cell during a time step must not exceed the mass of vapor present in that cell [10].

$$\dot{q}_{\mathrm{lim,mass}} = -\frac{(1-\alpha)\rho_{\mathrm{V}}h_{\mathrm{LV}}}{\Delta t} \tag{11}$$

For numerical stability in an advection simulation, the CFL condition requires that the local velocity does not transport fields beyond one grid cell per time step ($u_{\mathrm{x}} < \Delta x/\Delta t$). Similarly, the condensation process in a mesh cell should not sink more volume than that of the cell per time step. This condition is ensured by limiting the local volumetric rate of volume sinking to $1/\Delta t$:

$$\dot{q}_{\mathrm{lim,CFL}} = -\frac{h_{\mathrm{LV}}}{\Delta t}\left(\frac{1}{\rho_{\mathrm{V}}} - \frac{1}{\rho_{\mathrm{L}}}\right)^{-1} \tag{12}$$

In an alternate approach, the simulation time step size could be adjusted dynamically to satisfy this CFL condition. However, this might lead to unnecessarily small time steps due to sharp temperature profiles from initial conditions or few relatively insignificant cells at the intersection of domain boundaries.

Thus, the limiting operation for condensation (where phase change heating is negative) can be defined as:

$$\dot{q}_{\mathrm{pc}} = \max\left(\dot{q}_{\mathrm{pc},0}\ ,\ \dot{q}_{\mathrm{lim,mass}}\ ,\ \dot{q}_{\mathrm{lim,CFL}}\right) \tag{13}$$

Once $\dot{q}_{\mathrm{pc}}$ is obtained for interface cells, the volumetric generation ($\dot{v}_{\mathrm{pc}}$) and phase fraction generation ($\dot{\alpha}_{\mathrm{pc}}$) terms can be evaluated.

$$\dot{v}_{\mathrm{pc}} = \frac{\dot{q}_{\mathrm{pc}}}{h_{\mathrm{LV}}}\left(\frac{1}{\rho_{\mathrm{V}}} - \frac{1}{\rho_{\mathrm{L}}}\right) \tag{14}$$

$$\dot{\alpha}_{\mathrm{pc}} = -\frac{\dot{q}_{\mathrm{pc}}}{\rho h_{\mathrm{LV}}} \tag{15}$$

ALGORITHM IMPLEMENTATION

The modeling approach for condensation developed in this investigation is implemented using the OpenFOAM® finite volume library [6], and is based on the packaged interFoam VOF solver [14]. OpenFOAM® provides implementations of many key components needed for continuum mechanics simulation including: mesh reading, differencing and upwinding schemes, linear system solvers, and algorithm parallelization, and enables intuitive definition of field operations and PDEs [26]. The interFoam solver supports adiabatic incompressible two-phase fluid-fluid flows without phase change. No geometric interface reconstruction or tracking is performed in interFoam; rather, a compressive velocity field is superimposed in the vicinity of the interface to counteract numerical diffusion. The condensation flow solver developed here adds a thermal energy transport equation, modifies the base equations with phase change terms, and provides support for generic phase-change models. Thus, phase-change models can be selected by the user during runtime, and new models can be rapidly incorporated.

At startup, the solver loads the mesh, reads in fields and boundary conditions, and initializes sub-models for two-phase fluid properties, turbulence (if selected), and the phase-change model. During this initialization stage, the condensation phase-change model constructs the graph of mesh-cell connectivity used to identify interface cells.

The main solver loop is then initiated. First, the time step is dynamically modified to ensure numerical stability. In the base interFoam solver, the time step is only adjusted to satisfy the CFL condition. Here, it is also corrected to ensure that the thermal diffusion stability condition is satisfied for all cells *i*:

$$\Delta t \le l \min\left[\Delta^2 \Big/ \left(\frac{k}{\rho c_{\mathrm{p}}}\right)_{\mathrm{eff}}\right]_{\mathrm{i}} \tag{16}$$

Here, l is a user-defined constraint (typically 1/4 or 1/6 in 2D or 3D simulations, respectively) and Δ is the minimum cell-edge length. This condition in not typically considered in fluid flow simulations, but is necessary for condensation simulations where thermal conduction plays a significant role and the mesh is finely graded near the interface.

Next, the two-phase fluid mixture properties and turbulence quantities are updated. The phase-change model is then evaluated, and the $\dot{q}_{\mathrm{pc}}$, $\dot{v}_{\mathrm{pc}}$, and $\dot{\alpha}_{\mathrm{pc}}$ fields are obtained.

The discretized phase fraction equation (Eqn. 6) is then solved for a user-defined number of sub-time steps (typically 2-3) using the multidimensional universal limiter with explicit solution (MULES) solver. This solver is included in the OpenFOAM library, and performs conservative solution of hyperbolic convective transport equations with defined bounds (0 and 1 for α).

Once the updated phase field is obtained, the program enters the pressure-velocity (PIMPLE) loop. First the matrix equation for the momentum equation is formed. Then an inner pressure-velocity correction loop (PISO) is initiated. In the PISO loop, an intermediate velocity field is first obtained, and the cell-face volume fluxes (ϕ) are evaluated and corrected for gravitational forces, the continuum surface tension force, and boundary conditions. The pressure-Poisson equation is then formed and solved. Following the approach of [26], the coefficients of the pressure equation are obtained from the diagonal entries of the momentum matrix equation ($1/\mathrm{A_D}$). For *incompressible* flows, the pressure equation would be:

$$\nabla\cdot\left(\frac{1}{\mathrm{A_D}}\nabla p_{\rho\mathrm{gh}}\right) = \nabla\cdot\phi \tag{17}$$

Here, $\nabla\cdot\phi$ is the numerical equivalent of the divergence of the velocity field ($\partial u_{\mathrm{i}}/\partial x_{\mathrm{i}}$) for a cell. As the pressure velocity loop is iterated, $\nabla\cdot\phi$ approaches zero, recovering the incompressible continuity condition. However, for the condensing flows investigated here, $\partial u_{\mathrm{i}}/\partial x_{\mathrm{i}} = \dot{v}_{\mathrm{pc}}$. Thus, the pressure equation becomes:

$$\nabla\cdot\left(\frac{1}{\mathrm{A_D}}\nabla p_{\rho\mathrm{gh}}\right) = \nabla\cdot\phi - \dot{v}_{\mathrm{pc}} \tag{18}$$

After the pressure equation is solved, the velocity field is corrected with the updated pressure field, and boundary conditions are updated. The pressure-velocity loops (PIMPLE and PISO) continue for a user specified number of iterations.

Finally, the thermal energy transport subsection is entered. First, the enthalpy field is reevaluated from the temperature field (Eqn. 9). Then, for a user-defined number of steps (typically 2-3), alternating solution of the energy equation (Eqn. 5) and update of the temperature field ($T(h)$) are performed. The actual evaluated thermal energy equation incorporates an artificial enthalpy diffusion term. This is added to avoid solution "checker-boarding," an effect that occurs when neighboring cells are decoupled in a first order differential equation, leading to alternating field values.

1. Initialize simulation data and phase change model
2. **WHILE** $t < t_{end}$ **DO**
    1. Update Δt for stability
    2. Update fluid and turbulence properties (ρ, μ_{eff}…)
    3. Update phase change model ($\dot{q}_{pc}$, $\dot{v}_{pc}$, $\dot{\alpha}_{pc}$)
    4. Phase equation sub-cycle
    5. **DO** PIMPLE
        1. Form *u* equation
        2. **DO** PISO
            1. Obtain and correct face fluxes (ϕ)
            2. Solve *p*-Poisson equation
            3. Correct *u*
        3. **LOOP**
    6. **LOOP**
    7. Update $h(T)$
    8. **DO** Energy Loop
        1. Solve *h* equation
        2. Update $T(h)$
    9. **LOOP**
3. **LOOP**

FIG. 2 – FLOW SOLUTION ALGORITHM SUMMARY

$$\left\{\frac{\partial}{\partial t}(\ )+\frac{\partial}{\partial x_i}(u_i\,\cdot)-\frac{\partial}{\partial x_i}\left[\left(\frac{k}{\rho c_p}\right)_{eff}\frac{\partial}{\partial x_i}(\ )\right]\right\}h = \frac{\partial}{\partial x_i}\left[\left(\frac{k}{\rho}\right)_{eff}\frac{\partial T}{\partial x_i}-\left(\frac{k}{\rho c_p}\right)_{eff}\frac{\partial h}{\partial x_i}\right]-\dot{q}_{pc} \quad (19)$$

In Eqn. 19, terms on the left side of the matrix equation are solved implicitly (indicated by the operator notation), and terms on the right side are applied explicitly.

The main solver loop iterates until program termination. A summary of the simulation algorithm is presented in Fig. 2.

VALIDATION STUDIES

Horizontal Film Condensation

The condensation phase-change model and solver developed here are first tested for grid independence and accuracy for horizontal film condensation – a configuration with relatively weak dynamic effects. In this case, a liquid film condenses on the top surface of an isothermal plate (at T_w) in a pure atmosphere. This is similar to the horizontal film validation studies conducted in [10, 21].

By assuming a linear temperature profile from T_w at the lower wall to T_{sat} at the interface, a control volume analysis leads to an analytical solution for the film thickness $\delta_{an}(t)$.

$$\delta_{an}(t)=\left[2t\left(\frac{k}{\rho c_p}\right)_L\left(\frac{1}{2}+\frac{h_{LV}}{c_{p,L}\Delta T}\right)^{-1}\right]^{1/2} \quad (20)$$

Here, the initial condition of $\delta(t = 0) = 0$ is assumed.

Isobutane at p_{sat}(25°C) is selected as the modeled fluid due to its moderate values of liquid-to-vapor property ratios and phase change enthalpy (ρ_l/ρ_v = 60.4, Ja = 0.037 for ΔT = 5 K). Relevant thermophysical properties for saturated isobutane at 25°C are summarized in Table 1.

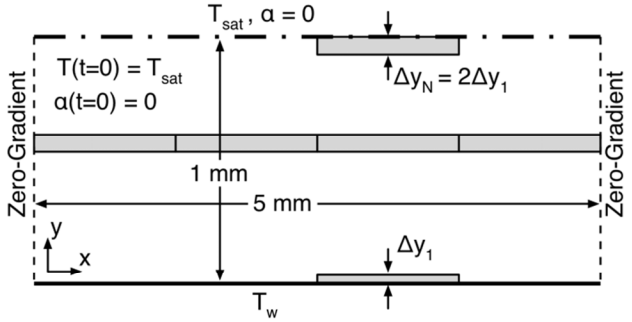

FIG. 3 – GEOMETRY FOR HORIZONTAL FILM CONDENSATION STUDIES

TABLE 1 – PROPERTIES OF SATURATED ISOBUTANE AT 25°C

Property	Liquid	Vapor
ρ (kg m^{-3})	550.6	9.12
μ (kg m^{-1} s^{-1})	$1.51\cdot10^{-4}$	$7.73\cdot10^{-6}$
k (w m^{-1} K^{-1})	0.089	0.017
c_p (kJ kg^{-1} K^{-1})	2.45	1.82
σ (kg s^{-2})	0.0099	
h_{LV} (kJ kg^{-1})	329.4	

A 2D rectangular domain is employed with horizontal and vertical dimensions of 5 mm and 1 mm, respectively. The mesh is defined with 4 uniform cells per horizontal row, and grading in the vertical direction with cells in the bottom row being half the height of the uppermost row. Zero-gradient boundary conditions are applied to the vertical sides of the domain. The bottom wall is set to T_w = 20°C, and the top "freestream" boundary is set to T_{sat} = 25°C. All fluid entering through the freestream boundary is vapor (α = 0). The domain is initialized with uniform conditions T = 25°C (T_{sat}) and α = 0 (all vapor). A schematic of the simulation domain is presented in Fig. 3.

The grid independence study is conducted for cases of N = 84, 112, 150, 200, and 267 rows in the y-direction. The simulation time step is modified dynamically following the method described in the algorithm implementation section. Results are recorded at every 0.02 simulation seconds (ss) for 5 ss.

The development of the liquid film thicknesses and relative errors are presented for representative cases in Fig. 4. Here, the film thickness is evaluated as the total liquid volume divided by the base area. While the analytical solution (δ_{an}) is independent of *x*, numerical solution leads to slight variations in the *x* direction.

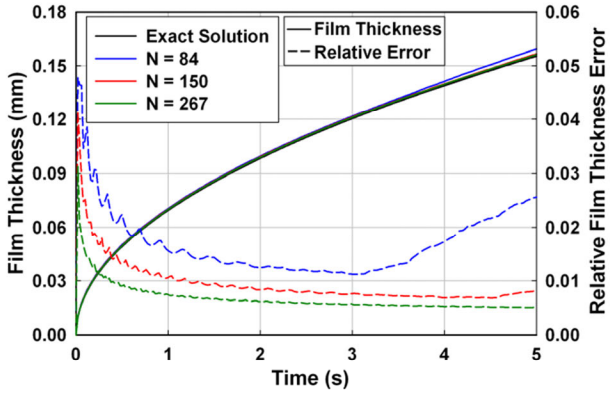

FIG. 4 – HORIZONTAL CONDENSING FILM DEVELOPMENT

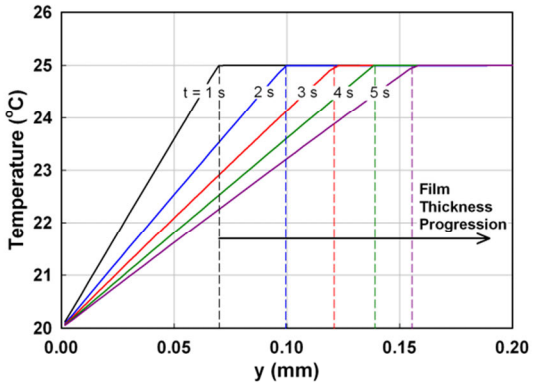

FIG. 5 – HORIZONTAL FILM TEMPERATURE PROFILES

Integrated simulation error can be estimated as the film thickness error ($|\delta_{sim}-\delta_{an}|$) summed over time steps i, weighted by Δt (0.02 s) (Table 2).

$$E = \sum_i \left|\delta_{sim} - \delta_{an}\right| \Delta t \tag{21}$$

TABLE 2 – HORIZONTAL FILM CONDENSATION CONVERGENCE

	Simulation (N)					
	84	**112**	**150**	**200**	**267**	**Exact**
$\delta(t = 5)$ (mm)	0.1594	0.1569	0.1566	0.1563	0.1562	0.1554
E (μm s)	8.51	5.25	4.32	3.61	3.11	

A power-law curve fit to these results data indicates that the total error for the condensation study scales with the mesh resolution as $E \propto \Delta y^{0.84}$ ($R^2 = 0.93$).

Representative vertical centerline temperature plots for the N = 200 case are presented in Fig. 5. These results indicate that linear temperature profiles from T_w to T_{sat} are obtained in the liquid film, in agreement with the analytical solution.

Smooth Falling-Film Condensation

Smooth laminar falling-film condensation on a vertical isothermal wall represents a phase-change configuration with more complex dynamics, but for which analytical solutions can still be obtained. Following the Nusselt analysis [13], the temperature varies linearly from T_w at the wall to T_{sat} at the interface, and the film thickness and velocity profiles are:

$$\delta_{an} = \left[\frac{3\Gamma\mu_L}{\rho_L(\rho_L - \rho_V)g}\right]^{1/3} \tag{22}$$

$$u_{an}(x) = \frac{3\Gamma}{\rho_L\delta}\left[\frac{x}{\delta} - \frac{1}{2}\left(\frac{x}{\delta}\right)^2\right] \tag{23}$$

Here, Γ is the film mass flow per unit width of the vertical plate (kg m^{-1} s^{-1}).

The condensation simulations are conducted in a 2D rectangular simulation domain (~2.5 mm wide × ~25 mm tall). A thin guide vane (50 μm wide by 0.25 mm tall) is positioned so that the inlet film thickness corresponds to the value obtained from Eqn. 22. The guide vane is employed to avoid numerical instabilities that can arise if the liquid-phase fixed-velocity and vapor-phase zero-velocity-gradient boundary conditions are specified on adjacent mesh faces. The wall temperature is set to T_w (20°C), and the vapor boundaries (top and freestream) are set to T_{sat} (25°C). The guide vane and outlet sections are modeled as zero temperature gradient (adiabatic) surfaces. The liquid inlet flow is specified using the analytical temperature (linear) and velocity (Eqn. 23) profiles. The vapor boundaries are set with zero-gradient velocity and inlet $\alpha = 0$ (vapor) conditions. The bottom outlet is set with zero-gradient α and u conditions. A rectilinear mesh is employed with fine cells in the region of the film and guide vane (Δx = 3 μm, Δy = 11 μm for min(δ_{an}) = 66.4 μm). In the vapor bulk region, cells are graded in the x-direction, becoming coarser towards the freestream. A schematic of the falling-film condensation domain and initial conditions is presented in Fig. 6A.

As before, fluid properties correspond to saturated isobutane at 25°C. A range of inlet liquid flow rates and film thicknesses is selected corresponding to Re_f = 50, 100, 200, 400, 800, 1600 ($Re_f = 4\Gamma/\mu_L$). The falling-film condensation simulations are conducted for 0.5 seconds with values recorded at 0.025 s intervals.

For the six cases considered, the average wall heat fluxes agree with those obtained from the Nusselt analytical solution [13] to within a relative error of 0.021. Results for average wall heat fluxes are summarized in Table 3.

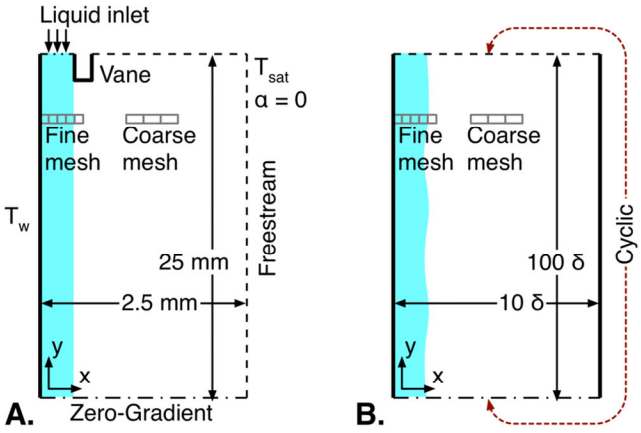

FIG. 6 – SMOOTH (A) AND WAVY (B) FALLING FILM DOMAINS

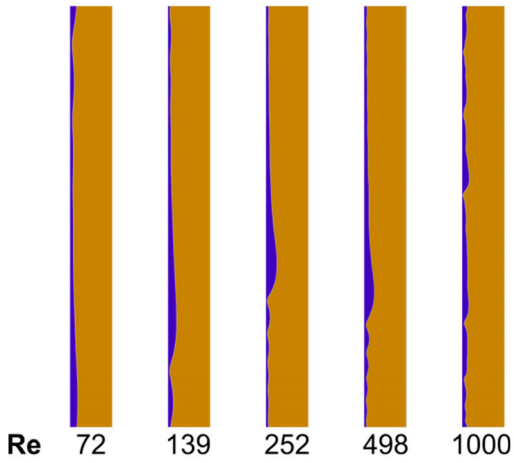

FIG. 7 – FULLY DEVELOPED WAVY FILM PROFILES

TABLE 3 – SMOOTH FALLING FILM HEAT FLUXES

	Film Reynolds Number					
Heat Flux	**50**	**100**	**200**	**400**	**800**	**1600**
Simulated (W m^{-2})	6608	5305	4234	3364	2654	2107
Analytical (W m^{-2})	6471	5254	4211	3356	2668	2119
Relative Error	0.021	0.010	0.005	0.003	0.005	0.006

Wavy Falling Film Condensation

More detailed analyses indicate that smooth falling films on vertical plates are inherently unstable [27], and wavy behavior is initiated at finite Reynolds numbers. Waves tend to generate thin film regions with reduced heat transfer resistance, yielding increased condensation rates [28].

Analytical solutions for wavy film profiles are not readily available. Thus, a set of adiabatic falling-film simulations was performed to obtain "fully developed" wavy conditions to provide inlet conditions for the condensation studies. For these studies, 2D rectilinear meshes were employed with wall conditions on the vertical boundaries. These studies were initialized with uniform stagnant films on the left wall with thicknesses (δ) corresponding to $\mathrm{Re_f}$ = 50, 100, 200, 400, and 800 (based on Eqns. 22-23). The right vertical wall was introduced to provide shear stress to the film interface, ensuring the development of waves. The top and bottom surfaces were mapped with *cyclic* boundary conditions for all fields, enabling the falling film to repeatedly flow through the domain so that slight interface disturbances could grow into fully developed waves. The mesh was graded finely near the left wall ($\Delta x = \delta/15$ for $x < 2.5\delta$) and more coarsely in the vapor bulk region with uniform $\Delta y = \delta/10$. The domain extents were scaled with δ as: $0 \le x \le 10\delta$ and $0 \le y \le 100\delta$. As before, fluid properties were selected to match saturated isobutane at 25°C. A schematic of the domain is presented in Fig. 6B.

A modified version of the interFoam [14] solver was employed for these simulations in which the hydrostatic term was removed from the velocity correction, and applied instead as an explicit source term in the momentum equation ($\bar{f}_B = (\rho_L - \rho)\bar{g}$). This approach allows pressure continuity across the cyclic top and bottom boundaries despite the hydrostatic difference.

The 5 wavy film cases were simulated for 1 ss. Final wavy film profiles for t = 1 ss are presented in Fig. 7.

Averaged $\mathrm{Re_f}$ values from ($0.5 \le t \le 1$ ss) based on liquid mass fluxes through the bottom surface at 0.0025 ss checkpoints are summarized in Table 4. For given $\overline{\mathrm{Re_f}}$, the

TABLE 4 – WAVY FILM REYNOLDS NUMBERS

Film thickness $\bar{\delta}$ (μm)	66	84	105	133	167
Nusselt $\mathrm{Re_f}(\bar{\delta})$	50	100	200	400	800
Simulation $\overline{\mathrm{Re_f}}$	72	139	252	498	1000

wavy film simulations predict lower $\bar{\delta}$ than the Nusselt model, consistent with the observations of [28].

Condensation studies are performed on the same meshes employed for the adiabatic wavy film simulations. The left wall is assigned a uniform surface temperature (T_w = 20°C). The right vertical boundary is modeled with a freestream condition at T_{sat}, to allow inflow of "makeup" vapor for the condensed fluid. Outflow (zero-gradient) conditions are applied to the bottom boundary. The inlet conditions (for α and u) to the top boundary are adopted from the outlet conditions of the adiabatic wavy simulation. A linear temperature profile from T_w to T_{sat} is applied to the top boundary to match the inlet film thickness. Initial conditions are mapped from t = 0.5 ss from the adiabatic studies, allowing waves to develop. The condensation simulations are performed for 0.5 ss.

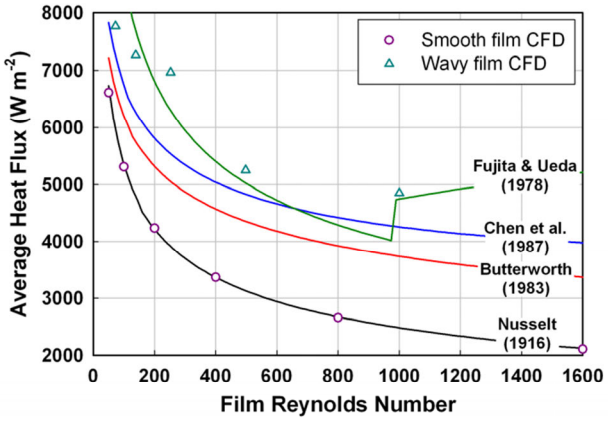

FIG. 8 – COMPARISON OF SIMULATION AND CORRELATION HEAT FLUXES

While exact solutions for wavy falling-film condensation heat transfer are not readily available, experimentally based correlations are available in the literature. Average heat fluxes obtained from the present simulations are compared with results from widely employed heat transfer correlations by Chen et al. [29], Butterworth [30], and Fujita and Ueda [31] (does not account for phase change) (Fig. 8). The heat transfer rates predicted using the Nusselt [13] solution are also reported for reference.

The simulated wavy film condensation heat flux values are generally higher than predictions from correlations. Overall trends of steeply decreasing $q(\mathrm{Re_f})$ at lower $\mathrm{Re_f}$ (72-498) and more gradual reduction at higher $\mathrm{Re_f}$ (498-1000) agree with results from [13, 29, 30]. Additionally, all simulation heat fluxes lie within 11% of the locus of results from these models. More rigorous comparison is difficult due to the wide range of experimental conditions analyzed to develop these correlations. Causes of discrepancies with correlations could include:

1. 3D effects – studies conducted on 2D meshes cannot account for 3D wave structures and dynamics
2. Long wavelength effects – simulation domains were 100δ in length, and thus suppress longer waveforms
3. Fully developed waves – simulated waves were allowed to grow to "fully developed" forms, and may differ from developing waves observed in condensation experiments
4. Assumed temperature profile – the assumed linear inlet temperature distributions in the films may differ from physical behavior

DISCUSSION

Evaluation of Condensation Model

Results from the horizontal film condensation studies indicate that the phase-change model developed here achieves grid independence at a nearly linear rate ($E \propto \Delta y^{0.84}$). While the approach of forcing interface cells to the equilibrium condition resembles that employed in earlier empirical rate parameter models ([8-10]), grid independence is obtained here by dynamically matching the condensation rate to the time step size. Agreement with theory and established correlations was found for the more complex case of falling film condensation, demonstrating the applicability of the model and solver to problems of engineering interest.

One limitation of the present condensation model is the assumption of negligible internal heat transfer resistance and thermal time scales of interface cells (i.e. $T = T_{sat}$, always, for interface cells). Thus, relatively fine meshes are required in the neighborhood of the interface for accurate phase change predictions. However, even adiabatic interface-capturing multiphase flow solvers (e.g. interFoam [14]) require fine meshes near interfaces to resolve effects such as surface tension and interfacial shear. Therefore, the net computational cost of applying this condensation model to a sufficiently resolved adiabatic simulation may be relatively small.

CONCLUSIONS

In this investigation, a thermally driven condensation phase-change model and solver was developed for VOF liquid-vapor flow simulations. This phase-change model operates on cell values, and thus does not require geometric interface reconstruction. The model was employed to study horizontal film condensation, and results were found to converge to analytical solutions nearly linearly with mesh resolution. Simulations of smooth and wavy laminar falling-film condensation on vertical plates were performed. Wall heat flux values for the smooth film cases were found to agree with analytical solutions to within 2%. Validation studies for wavy film condensation were less conclusive due to the wide range of heat transfer rates predicted by established correlations. Heat transfer rates obtained from the present study were found to lie within 11% of the locus of values obtained from commonly employed correlations, indicating general agreement.

In its present form, the model is limited to condensation cases. Future efforts will focus on extending it to evaporative phase change. Development of suitable boundary conditions for boiling is also of interest. With these advances, it is expected that reconstruction-free simulations can be performed for many liquid-vapor phase change processes of interest.

NOMENCLATURE

A_D	coefficient from momentum equation (kg m^{-3} s^{-1})
c_p	specific heat at constant pressure (kJ kg^{-1} K^{-1})
E	total simulation error (μm s)
f	volumetric forces (kg m^{-2} s^{-2})
g	gravitational acceleration (9.81 m s^{-2})
h	enthalpy (kJ kg^{-1} K^{-1})
i, j	indices
Ja	Jakob number ($c_{p,L}\cdot\Delta T/h_{LV}$) (-)
k	thermal conductivity (W m^{-1} K^{-1})
l	user defined time step constraint
N	number of mesh cells
P	pressure (Pa)
q	heat flux (W m^{-2})
$\dot{q}_{pc}$	volumetric phase change heating rate (W m^{-3})

r	empirical rate parameter in [8] (s^{-1})
Re	Reynolds number (-)
S	phase change rate in [8] (kg m^{-3} s^{-1})
t	time (s)
T	temperature (°C)
u	velocity (m s^{-1})
u^*	corrected (compressive) velocity (m s^{-1})
$\dot{v}_{pc}$	phase change volumetric generation rate (s^{-1})
x, y, z	principal axes

Greek Symbols

0	initial value
α	liquid volume fraction (-)
$\dot{\alpha}_{pc}$	liquid fraction generation rate (s^{-1})
Γ	mass flow per unit width (kg m^{-1} s^{-1})
δ	film thickness (m)
Δ	difference (ΔT, Δt) or cell size (Δ, Δx, Δy)
θ	thermophysical property
μ	dynamic viscosity (kg m^{-1} s^{-1})
ρ	density (kg m^{-3})
σ	surface tension (kg s^{-2})
τ	characteristic time scale (s)
ϕ	cell face volume flux (m s^{-1})

Subscripts

an	from (exact) analytical solution
B	body force
cell	mesh cell
eff	effective coefficent (can include eddy viscosity)
f	film property
int	property of interface
lim,mass	rate limited by mass availability
lim,CFL	rate limited by the CFL condition
L	liquid phase
LV	liquid-vapor property difference
n	normal to a surface (interface)
pc	phase change quantity
ρgh	for dynamic pressure (no hydrostatic component)
sat	saturated state
V	vapor phase

ACKNOWLEDGEMENTS

The authors wish to acknowledge generous financial support from the U.S. Department of Energy through the Krell Institute (contract DE-FG02-97ER25308), and computing resources from the National Energy Research Scientific Computing Center, which is supported by the Office of Science of the U.S. Department of Energy under (contract DE-AC02-05CH11231).

REFERENCES

1. Cavallini, A., Censi, G., Col, D. D., Doretti, L., Longo, G. A., Rossetto, L., and Zilio, C., 2003, "Condensation inside and Outside Smooth and Enhanced Tubes - a Review of Recent Research," *International Journal of Refrigeration*. **26**(4): pp. 373-392.
2. Thonon, B., 2008, "A Review of Hydrocarbon Two-Phase Heat Transfer in Compact Heat Exchangers and Enhanced Geometries," *International Journal of Refrigeration*. **31**(4): pp. 633-642.
3. *Ansys Fluent* 14.5, ANSYS, Inc., 2012.
4. *Ansys Cfx* 14.5, ANSYS, Inc., 2012.
5. *Comsol Multiphysics* 4.3a, COMSOL, 2013.
6. *Openfoam* 2.2.0, The OpenFOAM Foundation, 2013.
7. Hirt, C. W., and Nichols, B. D., 1981, "Volume of Fluid (Vof) Method for the Dynamics of Free Boundaries," *Journal of Computational Physics*. **39**(1): pp. 201-225.
8. Yang, Z., Peng, X. F., and Ye, P., 2008, "Numerical and Experimental Investigation of Two Phase Flow During Boiling in a Coiled Tube," *International Journal of Heat and Mass Transfer*. **51**(5-6): pp. 1003-1016.
9. Fang, C., David, M., Rogacs, A., and Goodson, K., 2010, "Volume of Fluid Simulation of Boiling Two-Phase Flow in a Vapor Venting Microchannel," *Frontiers in Heat and Mass Transfer*. **1**.
10. Thiele, R., 2010, *Modeling of Direct Contact Condensation with Openfoam*, Masters thesis in *Division of Nuclear Reactor Technology*, Royal Institute of Technology, Stockholm, Sweden, p. 46.
11. Jeon, S. S., Kim, S. J., and Park, G. C., 2009, "Cfd Simulation of Condensing Vapor Bubble Using Vof Model," *World Academy of Science, Engineering and Technology*. **60**: pp. 209-215.
12. Kim, S. J., and Park, G. C., 2008, *Interfacial Heat Transfer of Condensing Bubble in Subcooled Boiling Flow at Low Pressure*, in *Fifth International Conference on Transport Phenomena In Multiphase Systems*, Bialystok, Poland.
13. Nusselt, W., 1916, "The Surface Condensation of Water Vapour.," *Zeitschrift Des Vereines Deutscher Ingenieure*. **60**: pp. 541-546.
14. Weller, H. G., 2002, *Derivation Modelling and Solution of the Conditionally Averaged Two-Phase Flow Equations*, Nabla Ltd, Technical Report TR/HGW/02.
15. Rusche, H., 2002, *Computational Fluid Dynamics of Dispersed Two-Phase Flows at High Phase Fractions*, PhD Thesis in *Department of Mechanical Engineering*, Imperial College of Science, Technology & Medicine, London, UK, p. 343.
16. Bothe, D., and Warnecke, H. J., 2005, *Vof-Simulation of Rising Air Bubbles with Mass Transfer to the Ambient Liquid*, in *10th Workshop on Transport Phenomena in Two-phase Flow*. p. 61-72.
17. Rider, W. J., and Kothe, D. B., 1998, "Reconstructing Volume Tracking," *Journal of Computational Physics*. **141**(2): pp. 112-152.

18. Subramaniam, V., and Garimella, S., 2009, "From Measurements of Hydrodynamics to Computation of Species Transport in Falling Films," *International Journal of Refrigeration*. **32**(4): pp. 607-626.
19. Marschall, H., Hinterberger, K., Schuler, C., Habla, F., and Hinrichsen, O., 2012, "Numerical Simulation of Species Transfer across Fluid Interfaces in Free-Surface Flows Using Openfoam," *Chemical Engineering Science*. **78**: pp. 111-127.
20. Brackbill, J. U., Kothe, D. B., and Zemach, C., 1992, "A Continuum Method for Modeling Surface-Tension," *Journal of Computational Physics*. **100**(2): pp. 335-354.
21. Juric, D., and Tryggvason, G., 1998, "Computations of Boiling Flows," *International Journal of Multiphase Flow*. **24**(3): pp. 387-410.
22. Esmaeeli, A., and Tryggvason, G., 2004, "Computations of Film Boiling. Part I: Numerical Method," *International Journal of Heat and Mass Transfer*. **47**(25): pp. 5451-5461.
23. Tao, Y. J., Huai, X. L., and Li, Z. G., 2009, "Numerical Simulation of Vapor Bubble Growth and Heat Transfer in a Thin Liquid Film," *Chinese Physics Letters*. **26**(7).
24. Zhang, S. P., Ni, M. J., and Ma, H. Y., 2011, *Vof Method for Simulation of Multiphase Incompressible Flows with Phase Change*, in *Proceedings of the Sixth International Conference on Fluid Mechanics*, American Institute of Physics. p. 579-581.
25. Kissling, K., Springer, J., Jasak, H., Schutz, S., Urban, K., and Piesche, M., 2010, *A Coupled Pressure Based Solution Algorithm Based on the Volume-of-Fluid Approach for Two or More Immiscible Fluids*, in *V European Conference on Computational Fluid Dynamics*, Libson, Portugal.
26. Weller, H. G., Tabor, G., Jasak, H., and Fureby, C., 1998, "A Tensorial Approach to Computational Continuum Mechanics Using Object-Oriented Techniques," *Computers in Physics*. **12**(6): pp. 620-631.
27. Benjamin, T. B., 1957, "Wave Formation in Laminar Flow Down an Inclined Plane," *Journal of Fluid Mechanics*. **2**(6): pp. 554-574.
28. Jayanti, S., and Hewitt, G. F., 1996, "Hydrodynamics and Heat Transfer of Wavy Thin Film Flow," *International Journal of Heat and Mass Transfer*. **40**(1): pp. 179-190.
29. Chen, S. L., Gerner, F. M., and Tien, C. L., 1987, "General Film Condensation Correlations," *Experimental Heat Transfer*. **1**(2): pp. 93-107.
30. Butterworth, D., 1983, *Heat Exchanger Design Handbook*, E.H. Schlunder, Editor, Hemisphere, Washington, DC.
31. Fujita, T., and Ueda, T., 1978, "Heat Transfer to Falling Liquid Films and Film Breakdown I: Subcooled Liquid Films," *International Journal of Heat and Mass Transfer*. **21**(2): pp. 97-108.